JOURNAL OF GEOPHYSICAL RESEARCH, VOL. 104, NO. B6, PAGES 13,183–13,199, JUNE 10, 1999

Small-scale lateral shear velocity and anisotropy heterogeneity near the core-mantle boundary beneath the central Pacific imaged using broadband *ScS* waves

Sara A. Russell and Thorne Lay

Earth Sciences Department and Institute of Tectonics, University of California, Santa Cruz

Edward J. Garnero

Department of Geology, Arizona State University, Tempe

Abstract. Core-reflected *ScS* waves from 49 large ($M \geq 5.1$) deep Tonga-Fiji events, recorded in western North America are used to study a localized region of the core-mantle boundary (CMB) under the central Pacific Ocean. A total of 248 observations from the Berkeley Digital Seismic Network (BDSN), Caltech/United States Geological Survey (USGS) TERRAscope and the Incorporated Research Institutions for Seismology (IRIS) broadband arrays span epicentral distances of 73°-85°. *ScS* reflection points sample a CMB patch southeast of the Hawaiian islands at latitude 4° to 16° N and longitude -156° to -144° W, near the proposed source location of the Hawaiian plume. Highly variable *ScS* travel times, amplitudes, waveforms, and shearwave splitting indicate that the lowermost mantle in this region is heterogeneous both laterally and radially. *ScSH-SH* differential travel times are on average 4 s larger than predicted by the Preliminary Reference Earth Model (PREM). This is due to delayed *ScS* arrivals and is largely accounted for by a model with a strong velocity decrease in D". The *ScSH-SH* residuals also show a spatial trend not accounted for by a radial model, indicating a lateral decrease in lower mantle shear velocity to the northeast. This lateral velocity gradient appears to cause focusing of *ScS* energy. *ScSH/SH* amplitude ratios are larger than predicted by PREM or by a model with a strong negative gradient with depth in D", which enhances *ScS*. *ScS* splitting, corrected for lithospheric anisotropy beneath the receivers, indicates spatial variations in D" anisotropy with a systematic change in the orientation of the fast polarization direction from transverse to the ray path (fast *ScSH*) to parallel to the ray path (fast *ScSV*) along a northeast traverse. These spatial trends suggest lateral gradients in the boundary layer shear flow on scale lengths of a few hundred kilometers, which may be related to dynamical flow near the near the root of the large Hawaiian plume.

1. Introduction

The D" region, the lowermost few hundred kilometers of the mantle, plays a major role in the dynamics and chemical evolution of the Earth. D" serves as a dynamical, thermal, and chemical boundary layer between the molten iron alloy outer core and the crystalline lower mantle [*Knittle and Jeanloz*, 1991; *Loper and Lay*, 1995; *Wysession*, 1996; *Lay et al.*, 1997]. Heat, angular momentum, and possibly some material are exchanged across the core-mantle boundary (CMB), and changed across the core-mantle boundary (CMB), and thus an understanding of the physical nature of this region is fundamental to comprehending large-scale Earth processes such as mantle convection and the geomagnetic field. In addition, mantle plumes may originate from the CMB thermal boundary layer, giving rise to surface magmatism at hotspots [*Stacey and Loper*, 1983; *Olson et al.*, 1987; *Duncan and Richards*, 1991].

The central Pacific area examined in this study is known to have anomalous velocity structure in the lowermost mantle. Global seismic tomography models indicate that this region has slower than average shear velocity, in contrast to faster than average velocity characterizing D" beneath the circum-Pacific [*Tanimoto*, 1990; *Su et al.*, 1994; *Li and Romanowicz*, 1996; *Masters et*

Paper number 1999JB900114.
0148-0227/99/1998JB900114$09.00

al., 1996; *Grand et al.*, 1997; *Kuo and Wu*, 1997]. A shear velocity model, M1, with a near critical negative velocity gradient in the lowermost 200 km of the mantle has been proposed for this region [*Ritsema et al.*, 1997], and there is compelling evidence for a thin layer above the CMB, about 10-20 km thick, with strongly reduced velocities (5-10% decreases for P velocity and 15-30% for S velocity) [*Mori and Helmberger*, 1995; *Garnero and Helmberger*, 1996; *Revenaugh and Meyer*, 1997]. The low shear velocity is generally interpreted to indicate hotter than average temperatures, with the very large velocity reductions in the basal boundary layer suggesting the existence of partial melt in the hottest portions of the thermal boundary layer [*Williams and Garnero*, 1996].

Studies of travel times in localized regions show that there are significant small-scale velocity heterogeneities in D" that are not resolved by long wavelength global tomography. Small-scale (50-500 km) heterogeneities have been reported in numerous studies, including *Bataille et al.* [1990], *Gaherty and Lay* [1992], *Weber* [1993], *Wysession et al.* [1994], and *Lay et al.* [1997]. These results tend to support the large-scale patterns indicated by the long wavelength mapping [e.g., *Woodward and Masters*, 1991], but the small-scale features can be very strong and likely possess dynamical significance.

The complexity of the lowermost mantle is further revealed by recent studies of shear wave splitting that indicate the presence of anisotropy in the D" region [*Lay et al.*, 1998a, b]. Anisotropy in D" could arise from either development of lattice preferred orientations of minerals in strong shear flows [e.g., *Karato*, 1998] or from development of structural fabrics involving sheared chemical or partially molten heterogeneities [e.g., *Kendall and Silver*, 1996; *Lay et al.*, 1998b]. Shear waves with delays of the radial components with respect to the horizontal components have been found traversing paths beneath the central-eastern and southwest Pacific, Caribbean and the circum-Pacific regions [*Vinnik et al.*, 1995; *Kendall and Silver*, 1996; *Matzel et al.*, 1996; *Garnero and Lay*, 1997; *Ritsema et al.*, 1998, *Vinnik et al.*, 1998]. This is usually interpreted as evidence for transverse isotropy in these regions, although azimuthal sampling is very limited. Evidence for general anisotropy with small-scale variations has been presented by *Ritsema et al.* [1998] and *Pulliam and Sen* [1998], from analyses of D" under the central Pacific using diffracted shear waves.

In this study, we concentrate on a localized region near the CMB, southeast of the Hawaiian islands, that is sampled by shear waves from Tonga-Fiji earthquakes recorded by the dense broadband seismic arrays in western North America. ScS travel time, amplitude residuals, and splitting measurements indicate small-scale lateral gradients in structure near the CMB over scale lengths of 300-600 km [*Russell et al.*, 1998]. We consider the possibility that these structures are related to shear flow in the boundary layer associated with the base of the Hawaiian mantle plume.

2. Data

Our data set involves 49 earthquakes in the Tonga-Fiji subduction zone region recorded at 36 stations of the digital Caltech/United States Geological Survey (USGS) TERRAscope, Berkeley Digital Seismic Network (BDSN), and Incorporated Research Institutions for Seismology (IRIS) broadband arrays. The hypocenters are located from 180 to 637 km in depth and event magnitudes are between 5.1 and 7.6. Events with relatively simple waveforms and stable SH radiation patterns were selected in order to prevent source rupture complexities from obscuring deep mantle arrivals. Table 1 lists event information from the National Earthquake Information Center (NEIC). All of the records used are in the distance range of 73° to 85°, a favorable distance range for measuring $ScSH$-SH differential times and for seeking any lower mantle triplication arrivals [e.g., *Lay and Helmberger*, 1983]. The source-receiver geometries are displayed in Figure 1, with the portions of the ScS paths in the lowermost 270 km of the mantle indicated by darker line segments. Figure 2 illustrates S and ScS ray paths for an epicentral distance of 75° computed for shear velocity model M1, which was developed for the lower mantle beneath the central Pacific [*Ritsema et al.*, 1997]. The 248 ScS reflection points in our data span a 12° by 12° region at the CMB, providing a sampling density not typically achieved in D" studies.

The data processing included rotation of the horizontal traces to separate radial (SV) and tangential (SH) displacement components and band-pass filtering between 5 and 100 s to enhance the signal-to-noise ratio. Seismogram profiles were plotted to determine the degree of complexity of the waveforms and to detect any possible shear wave triplication arrivals, Scd, between S and ScS, which would indicate the presence of a D" discontinuity. Figure 3 shows a data profile, aligned on the S arrival, of a M=6.4 event on October 6, 1995, recorded at 17 stations. The traces illustrate the variability in ScS arrival times and waveforms on both the transverse and radial components for a single earthquake. Figure 3 also demonstrates the signal quality and sampling density characteristic of our data set. Figure 4 contains four examples of S wave traces recorded in Oroville, California, from different events. Note that the arrivals in both Figures 3 and 4 are impulsive, with good signal-to-noise ratios. There is little difficulty in identifying the major arrivals in this time window (S, SKS, and ScS) after allowing for systematic 4-5 s delays relative to model PREM [*Dziewonski and Anderson*, 1981]. The focal mechanisms, obtained from the Harvard CMT catalog, predict that ScS arrivals should have the same upward polarity on both components in Figures 3 and 4. Mild SKS contamination of the transverse components may

Table 1. Event Parameters[a]

Date	Time	Latitude	Longitude	Depth	Magnitude
May 20, 1990	0732:37.27	-18.10	-175.13	232	6.2
May 28, 1990	1128:47.69	-20.87	-177.99	486	5.9
June 8, 1990	1505:09.52	-18.87	-178.79	499	6.2
June 23, 1990	2138:18.75	-21.57	-176.48	181	6.5
June 26, 1990	1208:29.39	-22.02	-179.47	587	6.0
July 8, 1990	1630:02.14	-17.83	-178.90	560	5.3
July 22, 1990	0926:14.60	-23.62	-179.89	531	5.9
October 10, 1990	0554:53.54	-23.50	179.03	548	6.6
November 29, 1990	2058:11.08	-28.04	-179.71	415	5.1
April 18, 1991	0941:20.10	-22.92	-179.34	470	5.8
July 2, 1991	0608:09.00	-23.23	-179.13	429	5.7
September 30, 1991	0021:46.41	-20.88	-178.59	566	6.5
December 3, 1991	1033:39.92	-26.48	178.72	561	5.6
January 13, 1992	0937:43:70	-20.89	-178.74	575	5.9
February 20, 1992	1544:42.39	-15.38	-177.11	378	5.3
July 11, 1992	1044:19.76	-22.48	-178.41	377	6.4
August 4, 1992	0658:32.54	-21.74	-177.21	252	5.7
August 30, 1992	2009:05.77	-17.92	-178.71	565	5.8
November 12, 1992	2228:57.54	-22.40	-178.10	360	5.9
April 16, 1993	1408:38.93	-17.78	-178.86	565	6.9
April 20, 1993	1626:19.50	-20.88	-178.70	592	5.8
April 24, 1993	0954:21.20	-17.73	179.81	600	6.2
July 9, 1993	1537:53.65	-19.78	-177.49	398	6.1
August 7, 1993	1753:24.20	-23.87	179.85	523	6.7
August 21, 1993	0942:35.91	-21.28	-178.02	427	6.1
October 11, 1993	1307:29.56	-17.84	-178.73	555	6.0
November 10, 1993	1113:37.91	-15.34	-177.03	381	5.9
January 19, 1994	1626:48.06	-17.58	-178.50	533	6.1
March 9, 1994	2328:06.78	-18.04	-178.41	563	7.6
March 31, 1994	2240:52.15	-22.06	-179.53	580	6.5
April 18, 1994	2139:42.91	-21.41	-178.80	541	5.9
July 5, 1994	0259:42.41	-16.30	-177.47	414	5.9
August 11, 1994	1932:52.16	-21.84	-176.71	179	5.9
October 27, 1994	2220:28.54	-25.78	179.34	519	6.7
January 17, 1995	1654:11.81	-20.83	-179.24	634	6.3
April 13, 1995	0234:37.95	-13.45	170.43	638	6.2
August 25, 1995	1651:46.60	-18.69	-175.41	225	6.0
September 14, 1995	1224:34.18	-17.62	-178.97	533	5.9
September 18, 1995	2022:13.95	-20.64	-178.54	617	5.6
October 6, 1995	1139:34.81	-20.00	-175.92	198	6.4
October 29, 1995	1940:57.92	-21.79	-179.39	618	5.7
July 20, 1996	0741:15.29	-19.82	-177.64	356	5.7
August 5, 1996	2238:22.09	-20.69	-178.31	550	7.4
August 27, 1996	0624:07.91	-22.57	-179.79	574	5.6
October 19, 1996	1453:48.78	-20.41	-178.51	590	6.1
November 5, 1996	0941:34:77	-31.16	179.99	369	6.0
November 17, 1996	2111:20.27	-22.20	-179.70	591	5.5
December 1, 1996	2309:41.00	-30.52	-179.68	354	5.4

[a]from the National Earthquake Information Center

indicate lithospheric anisotropy, and clearly some of the *ScSV* arrivals have earlier peaks than the *ScSH* signals (events on October 6, 1995, and July 20, 1996), which is not accompanied by shifts of *SV* relative to *SH*. This suggests that part of the shear wave splitting occurs in the lowermost mantle where *ScS* diverges from *S*.

The signals have additional weak arrivals that vary from trace to trace, suggesting that they result from noise or event complexity. While some energy between *S* and *ScS* may correspond to lower mantle triplication arrivals, these extra arrivals are much more variable than observed beneath circum-Pacific study areas, and the existence of any discontinuity in D" requires analysis outside the scope of this paper. Our primary probes of the D" structure, for this study, are the *ScS* travel times, amplitudes, and shear wave splitting.

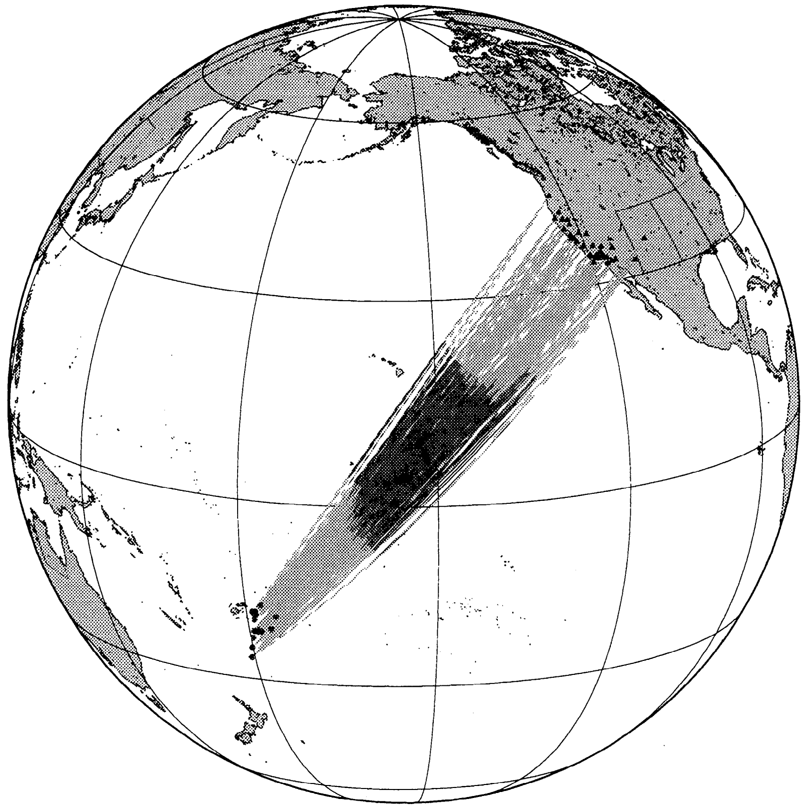

Figure 1. Great-circle paths of rays from sources in the Tonga-Fiji region (circles) to BDSN, TERRAscope, and IRIS broadband stations in western North America (triangles). The ray path segments for *ScS* phases within the lowermost 270 km of the mantle are the darker line segments, with the CMB reflection points approximately at the center of the segments.

3. Differential Time Analysis

We measured *ScSH-SH* differential times from 248 seismograms with clear arrivals. The measurements were made on the tangential components to avoid interference with *SKS* and because the tangential components have simpler waveforms. Seismograms with high noise levels or irregular *S* and *ScS* waveshapes were excluded. In the differential time calculations, we averaged the differences between onset and peak arrival times for the *S* and *ScS* phases. Noise often obscured the onsets, introducing uncertainty into the differential measurements. We estimate that there is a ± 0.5 s uncertainty in these measurements based on comparisons with waveform cross correlations. Cross-correlation results were not used because the waveshapes of *S* and *ScS* vary significantly in many cases.

Figure 5 shows the *ScSH-SH* differential time anoma-

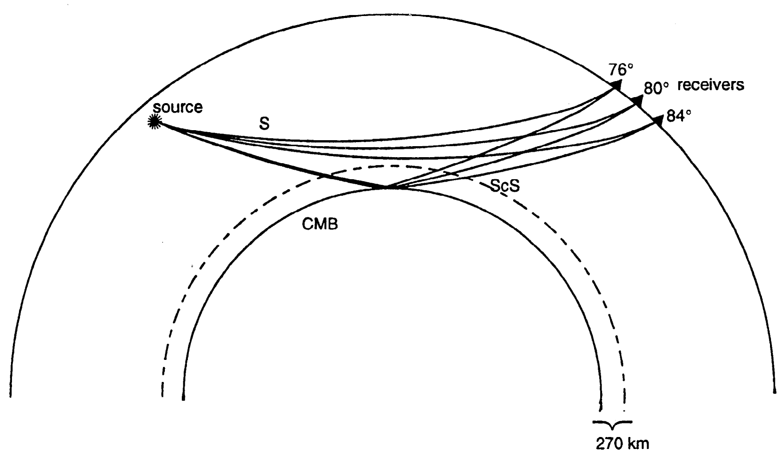

Figure 2. S and *ScS* ray paths at epicentral distances of 76° – 84° computed for model M1 [*Ritsema et al.*, 1997] for a 400 km deep source. *ScS* reflects off the core-mantle boundary while direct *S* turns in the mid-mantle. The *S* phase is used as a reference to *ScS* to suppress common heterogeneities on their similar ray paths through the upper mantle.

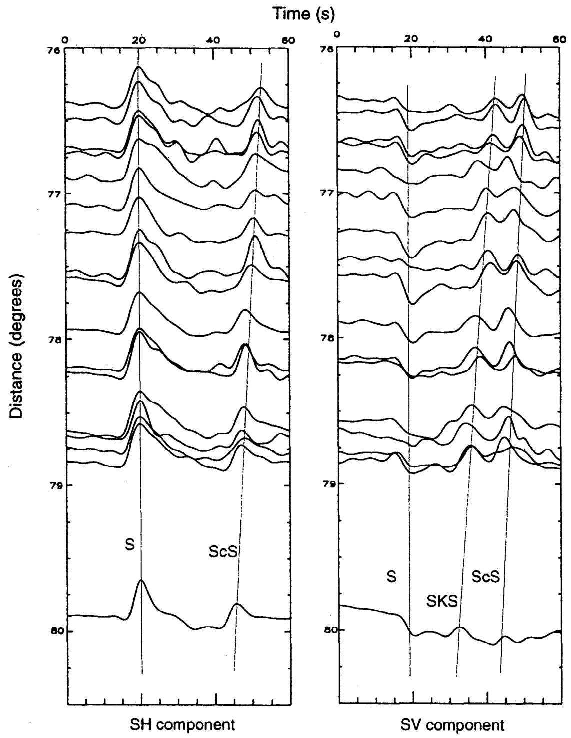

Figure 3. Transverse (left) and radial (right) waveform profiles of M=6.4 event on October 6, 1995, recorded on the BDSN and TERRAscope stations. The traces are aligned on the S phase. Peaks of the S and ScS arrivals are indicated by the lines. The traces are filtered with a phaseless Butterworth band-pass filter between 5 and 100 s. Note the variability in waveform shape and arrival time and also the lack of a coherent D" triplication arrival between the S and ScS phases.

lies with respect to PREM, after correction for ellipticity and adjustment of the distance to correspond to a source depth of 400 km. We define the differential time residual as

$$\delta T_{ScS-S}^{(PREM)} = \Delta T_{ScS-S}(observed) - \Delta T_{ScS-S}(PREM)$$

There is a large amount of scatter in the anomalies with a positive shift of about 4 s. This requires either early S arrivals, late ScS arrivals, or some combination. The scatter may be caused in part by topography at the CMB, strong lateral gradients in upper mantle structure underneath the sources and/or receivers, erroneous arrival time picks, or, as we will argue, strong heterogeneity in the deep mantle.

Given that tomographic models indicate slower than average mid-mantle and deep mantle shear velocity structure under the central Pacific, late ScS phases are the most likely cause of the baseline shift in Figure 5. To test this, we correlated $\delta T_S^{(PREM)}[T_S(observed) - T_S(PREM)]$ and $\delta T_{ScS}^{(PREM)}[T_{ScS}(obs) - T_{ScS}(PREM)]$ anomalies with the $\delta T_{ScS-S}^{(PREM)}$ differential residuals [e.g., *Lay*, 1983; *Lavely et al.*, 1986], where $T_{S,ScS}$ denotes absolute travel times for data (using NEIC hypocentral parameters) or a model. Figure 6 presents these correlations. The $\delta T_S^{(PREM)}$ correlation value of -0.15 is low compared to the $\delta T_{ScS}^{(PREM)}$ correlation of 0.63. The ScS anomalies also span a larger range than the S anomalies in Figure 5. The correlation of $\delta T_{ScS}^{(PREM)}$ with $\delta T_{ScS-S}^{(PREM)}$ indicates that the differential travel time anomalies are primarily the result of late ScS phases.

We compare the observed differential times with shear velocity models proposed for the deep mantle under the Pacific to help interpret the observations. The first comparison is with model M1 of *Ritsema et al.* [1997] which is characterized by a 0.2% shear velocity reduction from PREM at 2700 km depth and a 3% velocity reduction at 2891 km depth (Figure 7). This model was derived using diffracted shear wave times and amplitudes referenced to *SKS*. M1 accounts for up to 3.5 s of the baseline shift relative to PREM, due to delayed ScS arrivals. Figure 8 shows the observed residuals referenced to M1, δT_{ScS-S}^{M1}, adjusted in distance to correspond to a source depth of 400 km. There is less than a 1 s baseline shift and little trend with distance. The scatter is large and requires small-scale variations in S or ScS. A high-resolution tomographic model available for this region is from *Grand et al.* [1997]. This model has 2% low shear velocity in the area sampled by our ScS phases, with little variation from PREM predicted for S. We raytraced through the three-dimensional model, finding that ScS-S times are predicted to be 2-3 s larger than for PREM, which is somewhat less than predicted by M1. The scale length of variations in the tomographic model is greater than 500 km, and less than 1 s of variability about a one-dimensional model is predicted for ScS-S differential times with our geometry. This is illustrated in Figure 8, where ScS-S anomalies computed for the Grand model for each path in our data set are referenced to model M1. It is apparent that the lower mantle sampled by our data possesses velocity heterogeneity at smaller-scale lengths than resolved in available tomographic models.

The $\delta T_{ScS-S}^{(M1)}$ residual times are plotted at the CMB ScS reflection points in Figure 9, which shows that there is a spatial trend in differential residuals with respect to M1 with increasing values to the northeast. This trend is most discernible when the differential values are smoothed with a Gaussian cap average which highlights the longer wavelength trends. This may be more representative of the actual structure given the fact that the residuals accumulate along the lowermost mantle propagation path rather than at a single point and also the Fresnel zones of the waves are roughly 5° x 10° at the CMB, although the effective Fresnel zone might be much smaller [*Neuberg and Pointer*, 1995]. Because of the limited ray path coverage, the geometry of the heterogeneity cannot be constrained. If the shear velocity heterogeneity is concentrated in a 250 km thick D" layer, it requires lateral gradients of 3.5% in shear velocity over 600 km scale lengths to account for the range of variations.

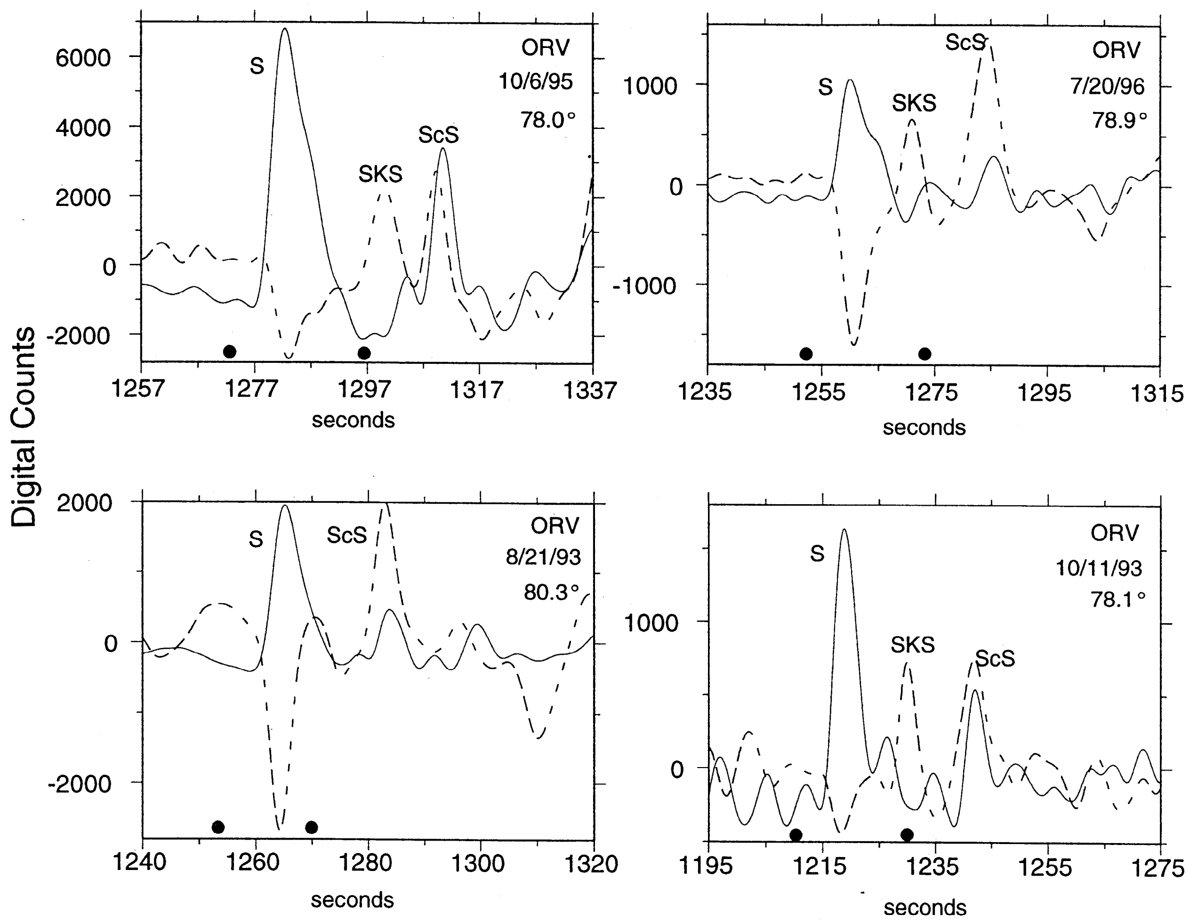

Figure 4. Four example broadband displacement shear wave recordings from the BDSN station ORV, in Oroville, California. The transverse (solid line) and the radial components (dashed line) are shown. The solid circles mark the predicted arrival times of the *S* and *ScS* phases for model PREM. The traces are filtered with a phaseless Butterworth band-pass filter between 5 and 100 s.

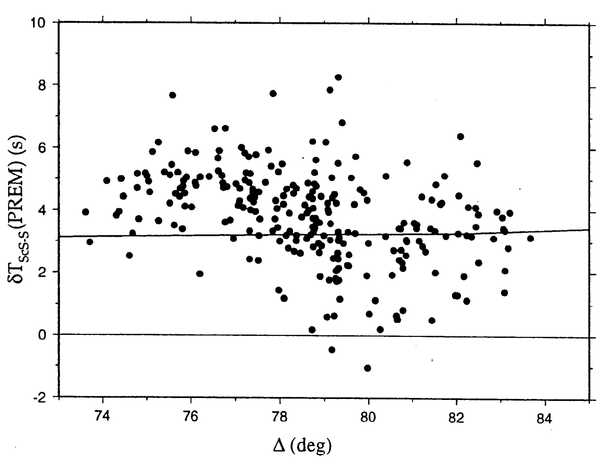

Figure 5. *ScSH-SH* residuals with respect to PREM plotted against epicentral distance. The observations are corrected to a common source depth of 400 km. The *ScSH-SH* differentials relative to PREM for model M1 [*Ritsema et al.*, 1997] is shown by the solid black line. The positive anomalies are consistent with observed *ScS* times 3-5 s late relative to PREM.

4. Amplitude Analysis

The amplitude of *ScS* is influenced by both attenuation and velocity structure. Examination of the seismograms reveals that *ScS* amplitudes fluctuate considerably. We measured the amplitude ratios of *ScSH/SH* on 236 seismograms, corrected for radiation pattern, and compared them to model predictions. The model amplitude ratios were measured on reflectivity generated synthetics for PREM and M1 using the PREM attenuation model. Peak-to-peak amplitudes were measured from band-pass filtered velocity traces, thus avoiding the baseline problems associated with displacement measurements.

A plot of log(*ScSH/SH* (obs)) - log(*ScSH/SH* (model)) versus great circle distance (Figure 10) indicates that the observed amplitude ratios are greater than predicted by both PREM (solid circles) and M1 (triangles). If the *S* wave amplitudes are assumed to be unaffected, then most of the observed *ScS* phases are anomalously large. This is contrary to the notion that *ScS* should

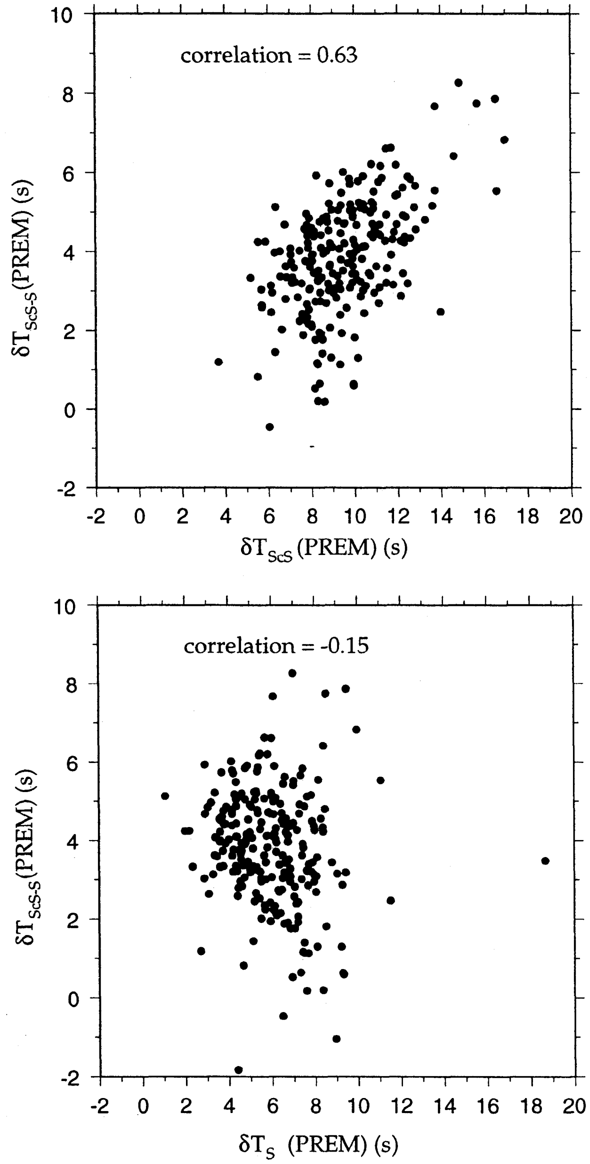

Figure 6. Absolute (top) *ScS* and (bottom) *S* residuals correlated with the *ScS-S* differential time residuals for PREM. Direct *S* has a lower correlation than the *ScS* phase suggesting that the large positive residuals accumulate along the isolated portion of the *ScS* ray path.

be strongly attenuated by traveling through the hotter than average structure suggested for this region. The strong negative gradient in model M1 focuses and amplifies *ScS*, thus it predicts the amplitude ratios slightly better than PREM. The *S* phases may be defocused or attenuated; however, owing to the difficulty of interpreting absolute amplitudes, we are unable to uniquely constrain which phase is responsible for the amplitude anomalies.

The *ScSH/SH* amplitude ratios referenced to model M1 are plotted at *ScS* CMB reflection points in Figure 11. Figure 11 (bottom) shows the logarithmic amplitude anomalies Gaussian cap averaged with a cap radius of 1.5°. The amplitude anomalies produce a patchy pattern and do not readily appear to correlate with the observed trends in travel time residuals (Figure 9). A low correlation value of 0.10 between the amplitude anomalies and the travel time residuals further establishes this point. Modeling the amplitudes presents many challenges, given the uncertainties in the elastic and anelastic structure. Therefore, in the remainder of this paper we will concentrate on the travel times of section 3 and the anisotropy analysis described in section 5.

5. Anisotropy Analysis

As noted earlier, there is evidence for shear wave splitting of *ScS* in our data set. This could arise anywhere along the *ScS* ray path. It is known that there is significant lithospheric anisotropy present beneath many stations in western North America [e.g., *Savage et al.*, 1990]. Anisotropic structure in the near-source slab environment is also a possibility which needs to be considered [*Fischer and Wiens*, 1996]. Finally, there is the possibility of deep mantle anisotropy which has been detected in D" in several regions [*Lay et al.*, 1998b]. The availability of models for lithospheric anisotropy allows us to apply a priori corrections to the *ScS* waveforms. We use splitting parameters tabulated by *Silver* [1996],

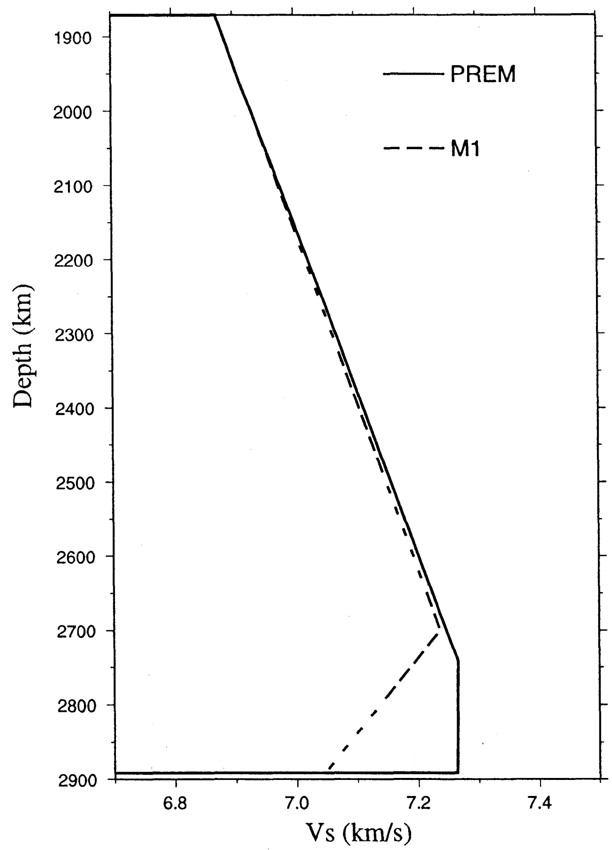

Figure 7. Shear velocity models of PREM [*Dziewonski and Anderson*, 1981] and M1 [*Ritsema et al.*, 1997] in the lower mantle. Model M1 was developed for the region directly to the northeast of our study area, based on diffracted shear waves.

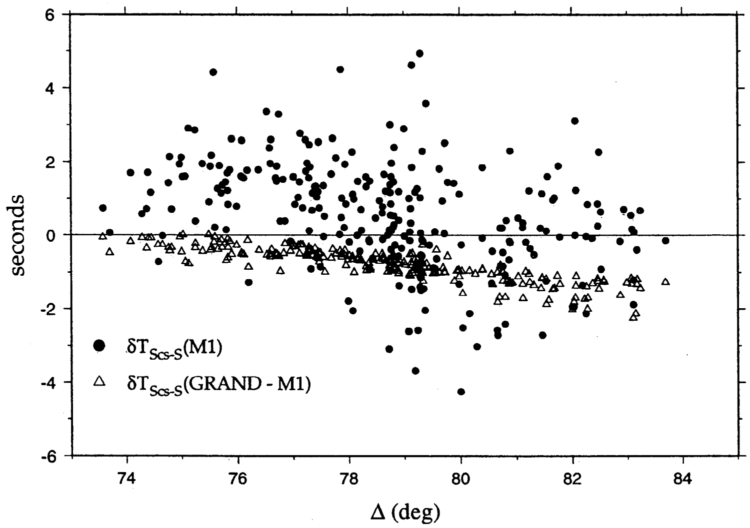

Figure 8. Comparison of $\delta^{(M1)}_{ScS-S(obs)}$ (circles) and $\delta^{(M1)}_{ScS-S(Grand)}$ (triangles) versus epicentral distance. The observations are corrected to a common source depth of 400 km. The *ScS-S* (Grand) differential times were calculated by raytracing through a three-dimensional tomographic model [*Grand et al.*, 1997] for our source/receiver geometries using M1 as a reference model. M1 accounts for much of the baseline shift relative to PREM in Figure 5, but large scatter remains. The tomographic model predicts only a small amount of scatter, and the data indicate more acute heterogeneity than contained in the model.

which are mainly derived from *SKS* waves that arrive with steep angles of incidence beneath the receivers. Our *ScS* phases arrive with very similar angles of incidence to those of *SKS*, thus the corrections are likely to be appropriate. We examined all observations for each station to ensure that a common station response was not left in the corrected data. In addition, a small time shift was applied to *ScSV* components to correct for a weak distance dependent phase shift in synthetic seismograms for our distance range, with a maximum value of approximately 0.2 s that results from the CMB reflection coefficient.

A subset of 84 seismograms was selected based on distinct onsets of *ScS*, clear waveforms on both the radial and transverse components, and availability of a lithospheric station correction. Seismograms in which *SKS* arrived within a few seconds of *ScSV* were eliminated.

To quantify any residual anisotropy after correction for the lithospheric models and CMB reflection, we used a correlation procedure [*Ansel and Nataf*, 1989] which rotated and shifted the radial and transverse components to find the optimal polarization angle and lag time. Because cross correlations are sensitive to zero crossings, we convolved the data with a long-period World-Wide Standardized Seismograph Network (WWSSN) response function. These correlation results were compared with results using the displacement records, and the measurement with the highest correlation value was used. When both had equally high correlations, the results were averaged. To ensure robust measurements, we also utilized the covariance method described by *Silver and Chan* [1991]. The anisotropy measurements that were consistent for both methods were retained. We estimate an uncertainty of 0.4 s in the splitting magnitudes and a 23° uncertainty in the polarization direction, based on the inverse *F* test [*Silver and Chan*, 1991]. Figure 12 shows six examples of uncorrected seismograms from three different earthquakes that illustrates the variability in anisotropy seen in the data The traces are aligned on the *S* phase with the hatchmarks signifying approximately the peaks of *ScSV* and *ScSH*. *ScSH* leads *ScSV* in GSC, in Goldstone, California, and SVD, in Seven Oaks Dam, California, and *ScSV* is the earlier arrival in the other four traces. Examples of a uncorrected and corrected seismogram are shown in Figure 13. The traces in the lower panel of Figure 13 were corrected for lithospheric anisotropy beneath the receiver and the small phase shift of *ScSV* at the CMB. Using both the correlation and covariance methods, a fast polarization angle of 77° and a split time of 0.4s was determined. Figure 14 depicts the measurement process along with the corresponding confidence region plot for a typical high-quality case.

The robust estimates of fast polarization directions and lag times are plotted at the CMB reflection points to detect any spatial systematics in the data. Figure 15 indicates the directions of the fast components of *ScS* with the length of the arrow representing the magnitude of the lag time. This plot reveals a change from fast directions transverse to the ray paths in the southwest to fast directions parallel to the ray paths in the northeast. The bimodal nature of the measurements is

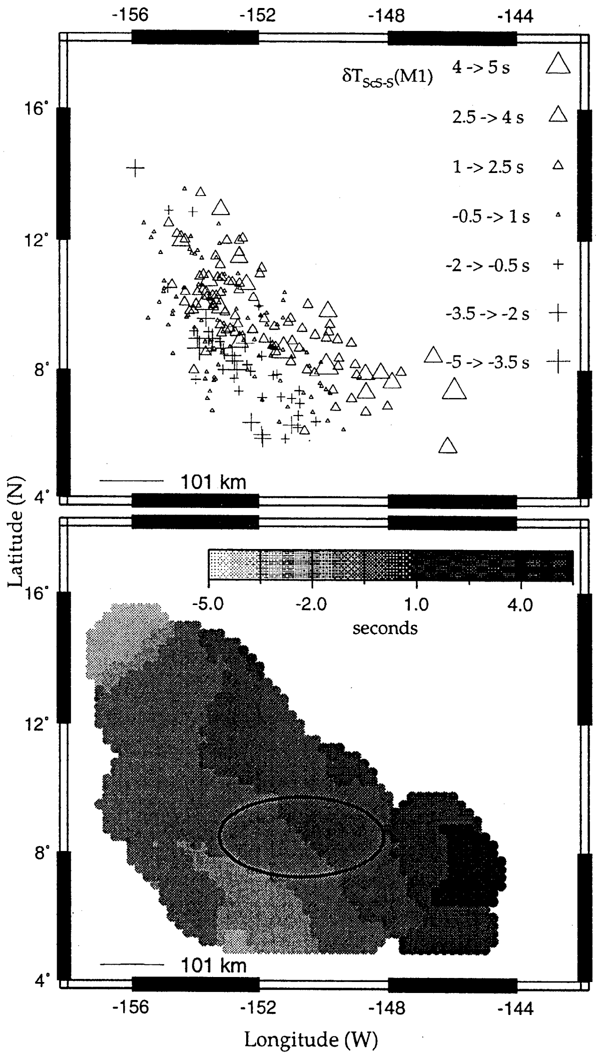

Figure 9. (top) *ScSH-SH* differential time residuals with respect to M1 plotted at the *ScS* reflection points on the CMB. (bottom) The same residuals smoothed with a Gaussian cap radius of 1.5°. This highlights a transition from small or negative residuals in the southwest portion of the region to larger more positive residuals to the northeast. The ellipse encompasses the proposed CMB locations of the base of the Hawaiian mantle plume from *Steinberger and O'Connell* [1998].

readily apparent, with a gradient in the direction of the fast polarization that is similar to that of the differential travel times.

It is important to recognize that the near coincidence of the great-circle path and the fast/slow polarization directions greatly simplifies the overall polarization of *ScS*, if it results from traversing an anisotropic layer at the base of the mantle. Depending on the geometry of anisotropy, the *ScS* phase may split into from two to four arrivals. Some of the null observations in Figure 15 may indicate intermediate states not well characterized by our bandwidth and polarization analysis. To assess the possibility that the trend in Figure 15 is created by the lithospheric receiver corrections applied to the data, we examined the splitting measurements at individual stations. Figure 16 shows the splitting measurements at each of the thirteen stations analyzed. The wide variability in lag times and polarization angles at each receiver verifies that the errors in lithospheric corrections are not generating the trends in the anisotropic values measured. Figure 17a presents splitting measurements from three stations plotted at the CMB that demonstrate that splitting measurements at individual stations are consistent with the anisotropic gradient seen in Figure 15, which arises from the entire population.

We also considered the possibility that near-source anisotropy is creating the trend in anisotropic polarization. To assess this prospect, we examined splitting measurements for individual events. Since the azimuth and *ScS* take-off angle are very similar for each station in a single event, because of our limited azimuthal and distance range (see Figure 2), the *ScS* waves should experience similar source-side anisotropy and thus exhibit similar polarization direction. Figure 17b shows splitting measurements for two events plotted at the CMB. Each event shows a range of spatially coherent polarization directions which indicates that source-side anisotropy is not creating the trend in *ScS* splitting. Another demonstration of this is provided by examining the polarization of *S* signals. If strong near-source anisotropy is present, one would expect both *S* and *ScS* to be affected. Figure 15 highlights the observations

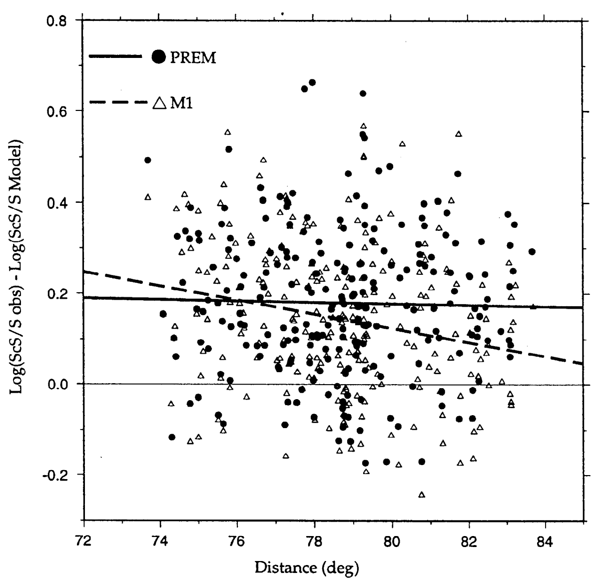

Figure 10. Plot of logarithmic *ScSH/SH* amplitude ratios normalized to PREM (circles) and M1 (triangles) versus epicentral distance. The amplitudes have been corrected for the source radiation pattern, and distances have been adjusted to a common source depth of 400 km. Positive values represent either larger than normal *ScS* or smaller than normal *S*. Model M1 predicts the amplitude ratios slightly better than PREM. The dashed (M1) and solid (PREM) lines represent the best fit line through the amplitude ratios.

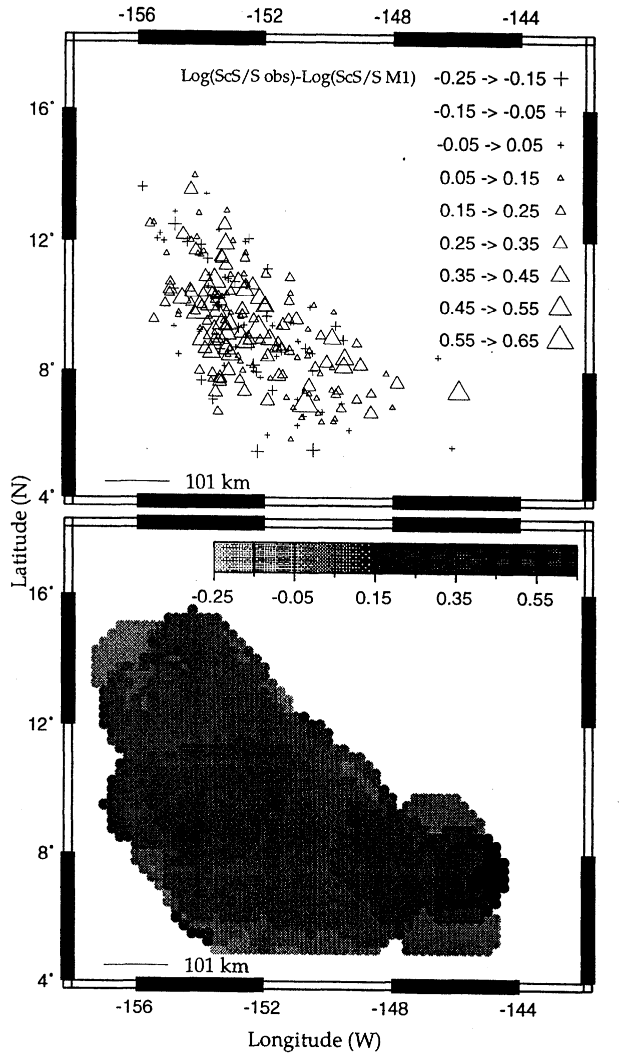

Figure 11. (top) Mercator map of logarithmic *ScSH/SH* amplitude ratios with respect to M1 plotted at the *ScS* reflection points on the CMB. (bottom) The same data but smoothed with a Gaussian cap radius of 1.5°.

with split *ScS* for which no *S* wave splitting was observed after correcting for anisotropy beneath the receiver. It is difficult to imagine how a near-source effect could produce the *ScS* pattern with no effect on *S*. There is no question that the lithospheric corrections and influence of source-side anisotropy are uncertain, but it seems improbable that a coherent trend would emerge out of individual and composite near-source and near-receiver effects that are not accounted for.

6. Discussion

The *ScS* travel times, amplitudes, and anisotropy measurements beneath the central Pacific indicate that the D" region is a highly heterogeneous region with small-scale gradients in intrinsic properties and associated dynamical processes. It remains an open question as to whether there is a shear velocity discontinuity at the top of D", as found beneath the circum-Pacific, Caribbean, Eurasia, Siberia, and India [e.g., *Lay and Helmberger*, 1983; *Zhang and Lay*, 1984; *Young and Lay*, 1987; *Weber and Davis*, 1990; *Gaherty and Lay*, 1992; *Ding and Helmberger*, 1997]. Studies by *Garnero et al.* [1988, 1993] indicated some evidence for a variable shear velocity discontinuity under the central Pacific, and *Reasoner and Revenaugh* [1999] have recently found evidence for a very weak *P* velocity discontinuity near 180 km above the CMB in our study area. An ongoing study favors the existence of a weak ($\leq 2.0\%$) shear velocity discontinuity near 200 km above the CMB, but the resulting triplication arrivals are less pronounced than in circum-Pacific regions.

The scale lengths involved in the travel time and anisotropy gradients are difficult to resolve given that the lack of crossing ray path coverage prevents tomographic imaging of the spatial extent of the heterogeneity. If the lateral variations are confined to within 250 km of the CMB, shear velocity variations of 3.5% over length scales of 600 km can account for the 3 s increase in *ScS* delays across our study region. Restricting the heterogeneous region to the lowermost 100 km of the mantle requires 7% lateral gradients over 300 km scale lengths, which would imply rather extreme lateral gradients. Either of these cases would require significant low-velocity regions embedded within an M1 type low-velocity zone. This may cause rapid focusing and defocusing of *ScS* amplitudes. Conversely, distributing the anomalous structure over greater depth extent toward the northeast from the CMB reflection points allows reduction of the magnitude of the velocity decrease. However, the study by *Ritsema et al.* [1997] provides some constraints on the amount of velocity variation to the northeast of the study region since any large decrease in shear velocity would affect the diffracted *S* phases that sample this locale.

The anisotropic gradients are likely to be located close to the CMB. Qualitatively, the bimodal behavior of the fast polarization directions shows the simplest spatial pattern, segregating arrivals with different polarization directions, when the measurements are projected at the *ScS* turning points. There is much more mingling of directions when the data are plotted at intersections with shallower depth surfaces. Observations by *Ritsema et al.* [1998] and *Pulliam and Sen* [1998] of direct *S* splitting for phases that sample the deep mantle northeast of our study area show intermittent cases of fast *SH* or fast *SV* as well as cases with no onset time splitting, which suggests that shear wave splitting does not accumulate in a simple way with pathlength toward the northeast. These factors favor an interpretation of strong lateral variations in anisotropy on lateral scale lengths of 300-500 km within the lowermost mantle. Lateral gradients of 2-3% in the magnitude of anisotropy and 90° changes in the fast polarization direction over scale lengths of 500 km are required if we confine the variations to a 100 km thick thermal

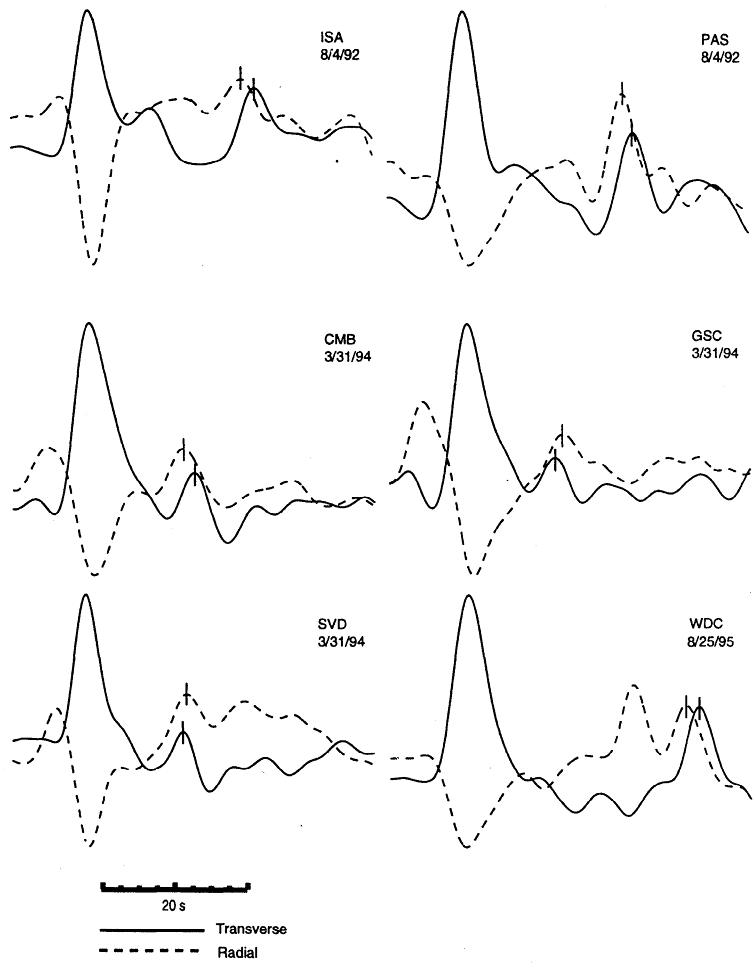

Figure 12. Six uncorrected seismograms, for earthquakes recorded on August 4, 1992, March 31, 1994, and August 25, 1995, that illustrate the large variability in *ScS* splitting. The traces are aligned on the *S* phase with the radial component shown as the dashed line and the transverse component shown as the solid line. The lines on the *ScS* phase show the peak arrival time. The traces PAS, in Pasadena, California, and SVD show cases where *ScSH* leads *ScSV*, while the remaining traces contain a fast *ScSV* phase.

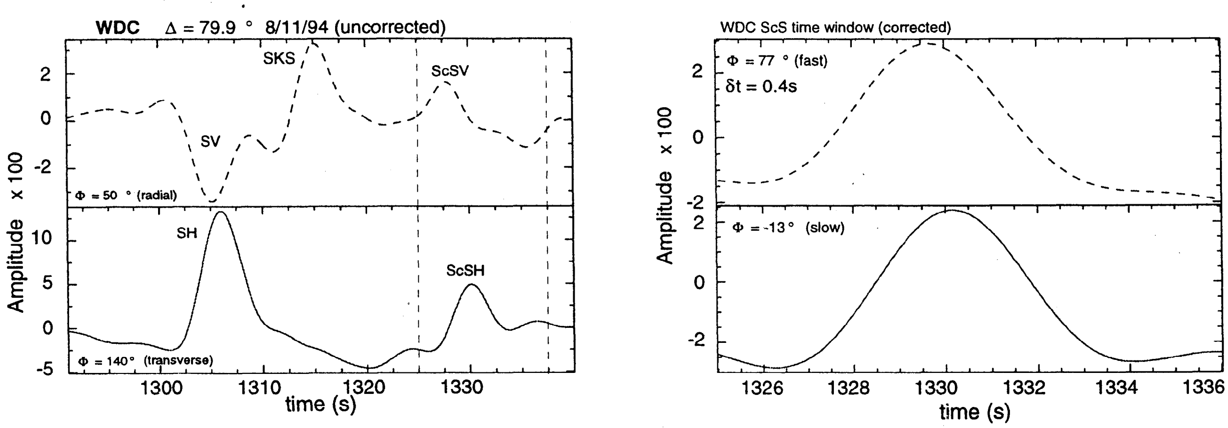

Figure 13. A seismogram from event August 11, 1994, recorded at station WDC, in Whiskeytown Dam, California, which shows evidence for shear wave splitting of *ScS*. (left) The uncorrected radial and transverse components of the *S* and *ScS* phases are shown. The vertical dashed lines denote the time window of the signals in the lower panel. (right) The windowed lithospheric and phase-shift corrected *ScS* phases rotated to the fast/slow polarization direction are shown. The covariance and correlation methods yield a fast polarization angle of 77°and a lag time of 0.4 s.

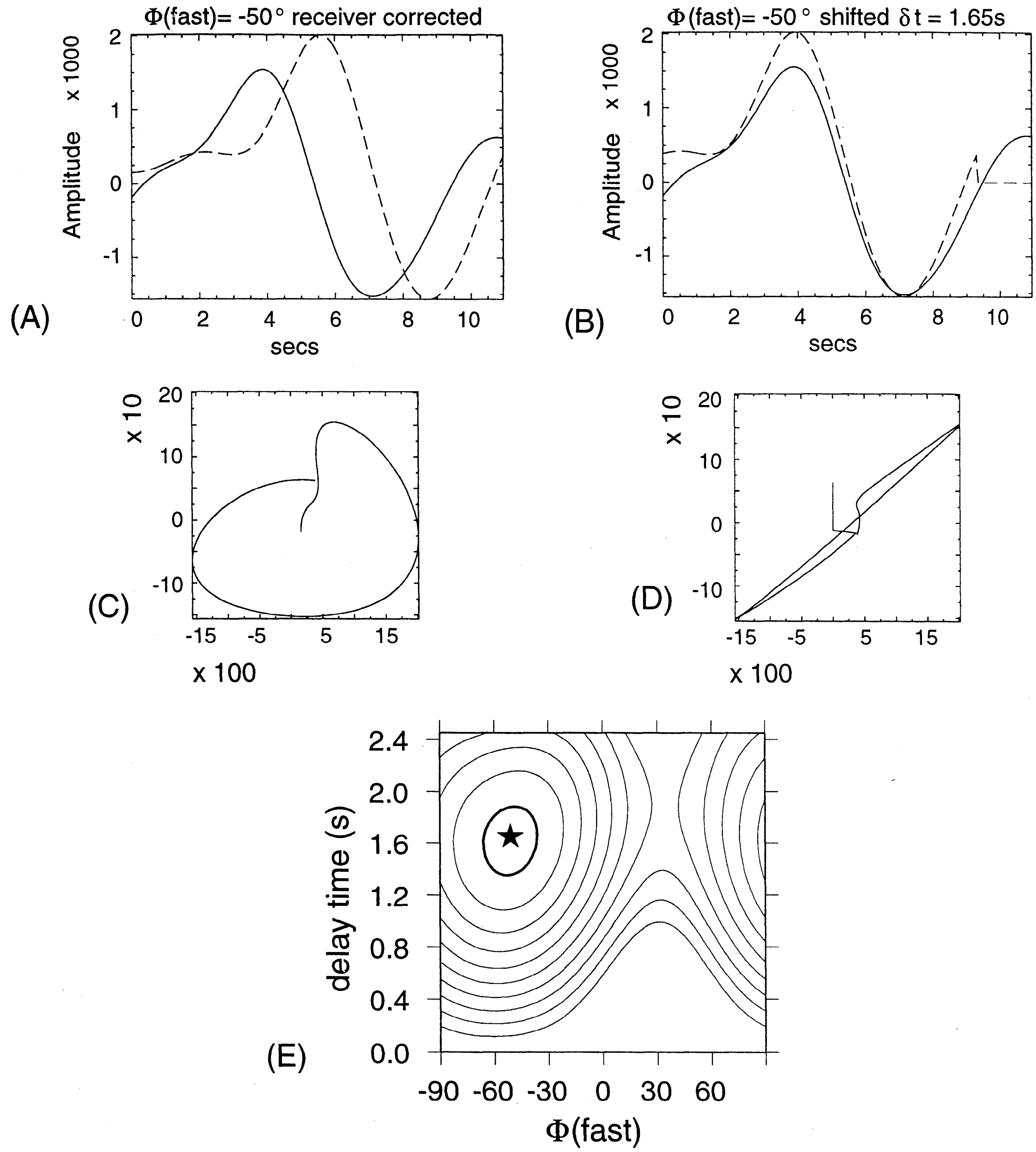

Figure 14. The receiver corrected seismogram and confidence region contour plot for station SVD on March 31, 1994 (original trace shown in Figure 12). (a) The *ScS* window lithospheric corrected, differentiated and rotated to the measured fast polarization direction. The fast component is indicated by the solid line. (b) The same trace with the slow component (dotted line) shifted by the measured delay time. (c,d) Particle motion plots, for Figures 14b and 14c, respectively, that display that the applied measured splitting corrections successfully linearize the *ScS* particle motion. (e) Confidence region contour plot as a function of fast polarization angle ϕ and delay time. The star marks the measured value with the surrounding darker contour indicating the 95% confidence region based on the inverse F test [*Silver and Chan*, 1991]. The succeeding contours are multiples of the 95% confidence region.

boundary layer at the CMB. Since these are sub-Fresnel zone scale lengths, it is difficult to constrain the actual structure, but Figures 9 and 15 provide a strong case for coupled lateral gradients in shear velocity (with *ScSH* slowing relative to *SH* toward the northeast) and anisotropy (with *ScSH* slowing relative to *ScSV* toward the northeast). While the geometry of the heterogeneous structure is not well resolved, our data clearly sample a low shear velocity region with strong lateral gradients involving decreasing velocities in the northeasterly direction.

The interpretation of our data as resulting from strong

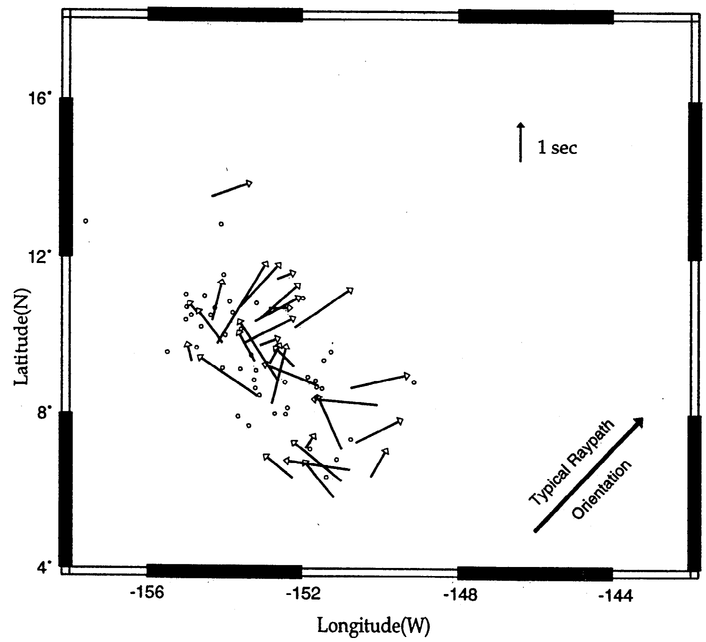

Figure 15. Mercator map showing fast polarization directions of ScS plotted at the ScS reflection points at the CMB. The length of the arrows represents the magnitude of splitting in seconds. The base of the arrows are located at the reflection point. Circles represent the reflection point locations of data with no splitting or with traces too noisy to obtain a reliable measurement. Black arrows represent measurements that possess no S splitting after the lithospheric correction was applied to the data. The bimodal nature of the values highlights a transition from fast directions perpendicular to the ray path direction in the southwest to fast directions parallel to the ray paths in the northeast.

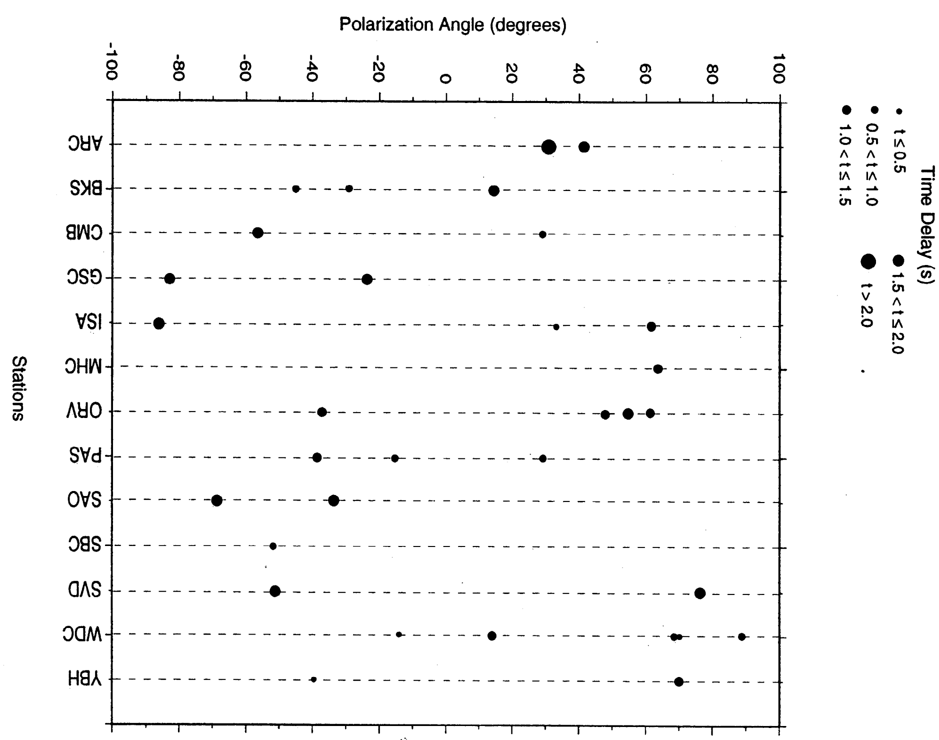

Figure 16. Fast polarization directions of ScS for the stations used in the anisotropy analysis. The symbols denote the measured amount of splitting in seconds. A wide variability of splitting angles and values can be seen at each receiver for ray paths that arrive at approximately the same azimuth and incidence angle with respect to one another.

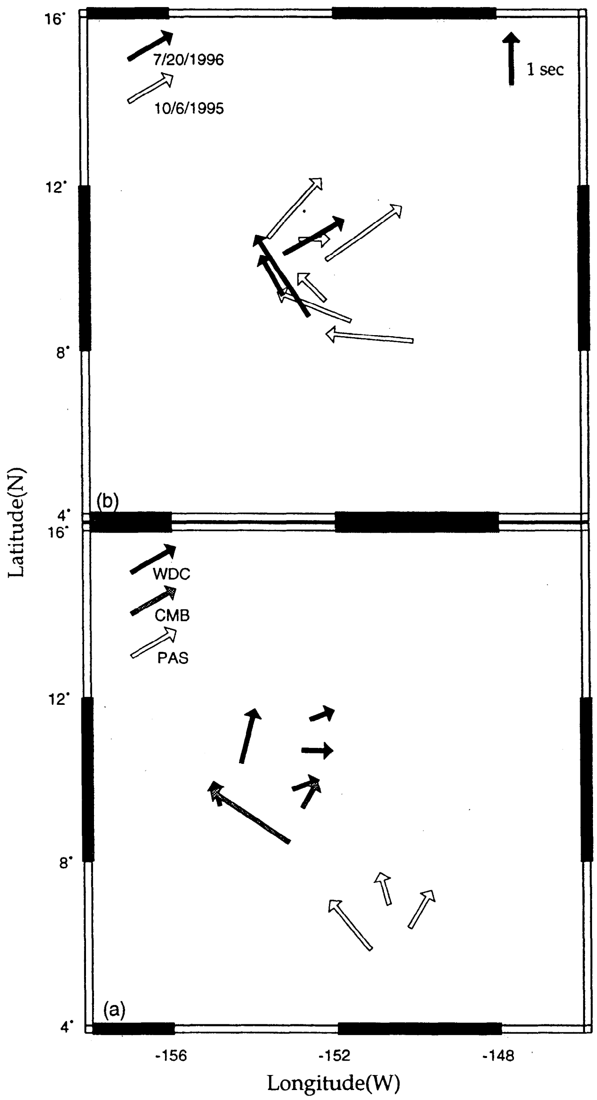

Figure 17. (a) Map of fast polarization directions of ScS measured at three stations, plotted at the ScS CMB reflection points. Station WDC is shown in black, CMB is shown in gray, and PAS is shown in white. The anisotropic gradient of fast directions perpendicular to the ray path direction in the southwest to fast directions parallel to the ray paths in the northeast is seen in the individual station values as well as in the combined measurements from all receivers (Figure 15). (b) Map of ScS fast polarization directions for events July 20, 1996 (black), and October 6, 1995 (white), plotted at the CMB. If source-side anisotropy is the cause of the anisotropic trend, then, since ScS ray paths have similar take-off angles and azimuths at the source, the polarization directions should be comparable. However, the variability of polarization direction in the individual events shows that the splitting measurements are not heavily influenced by source-side anisotropy.

small-scale heterogeneities in both shear velocity and anisotropy in the D" region beneath the central Pacific suggests a lateral change in physical properties and/or dynamic features. One possibility, though, which cannot be fully ruled out is that the gradients are related to the different areas of the source region that the ray paths sample. *Wysession et al.* [1994] address this question by noting that ScS-S and $sScS$-sS residuals, including residuals measured beneath the central Pacific, correlate well with one another. Since the surface reflected phases leave the source nearly perpendicular to S and ScS, a high correlation implies that common path heterogeneities are being suppressed. One might expect ScS phases to sample near-source high velocity slab material more extensively than S for the steeply dipping Tonga slab, which would predict early ScS arrivals rather than the late observations. Lacking reliable models of the slab shear velocity structure, we assume that the differential times and anisotropic measurements are not due to any source influences but rather are generated in the deep mantle.

There are several possible lower mantle scenarios that could explain the small-scale heterogeneities, including topography on the CMB and dynamical flows in the thermal boundary layer. CMB topography can produce ScS-S and ScS/S anomalies. *Murphy et al.* [1997] address this possibility after finding comparable scale length trends in PcP residuals mapped at the CMB beneath the eastern Pacific. They conclude that the calculated topography of an elevation range of 40 km over 700 km required to create 3 s residuals is too extreme. However, *Menke* [1986] shows that short-period PcP reflection amplitudes constrain topography in the CMB to be less than a few hundred meters. We conclude that topography cannot account for our 5 s residuals over approximately 600 km and also does not explain the observed accompanying transition in anisotropic directions.

Another conjecture is that the lateral gradients are caused by convective flow at the base of the mantle. Given the presence of a very low velocity zone at the base of the mantle in this region that appears to involve partial melt [*Williams and Garnero*, 1996; *Holland and Ahrens*, 1997] and the overall low velocity structure of D" in this region, the most likely explanation for our observations involves strong shear flow induced fabrics with inclusions of partial melt and/or chemical heterogeneity [*Sleep*, 1988; *Lay et al.*, 1998a]. Figure 18 illustrates a scenario in which the southwest portion of the region has strong horizontal shear flow containing entrained partial melt heterogeneities that smear laterally, producing either hexagonal symmetry with a vertical axis or preferred inclusion orientations such that $ScSH$ has a higher velocity than $ScSV$. In the northeast, an abrupt transition in the flow direction, possibly into an upwelling, could cause vertical alignments that make $ScSV$ the faster component. It may also be viable to have lattice preferred orientation in D" minerals produce the anisotropic structure, with a similar gradient in slow directions. As the nature of heterogeneities, mineralogy, deformation mechanism, and stress state are all unknown, it is not yet possible to quantify this scenario. However, the scale length of the transition in

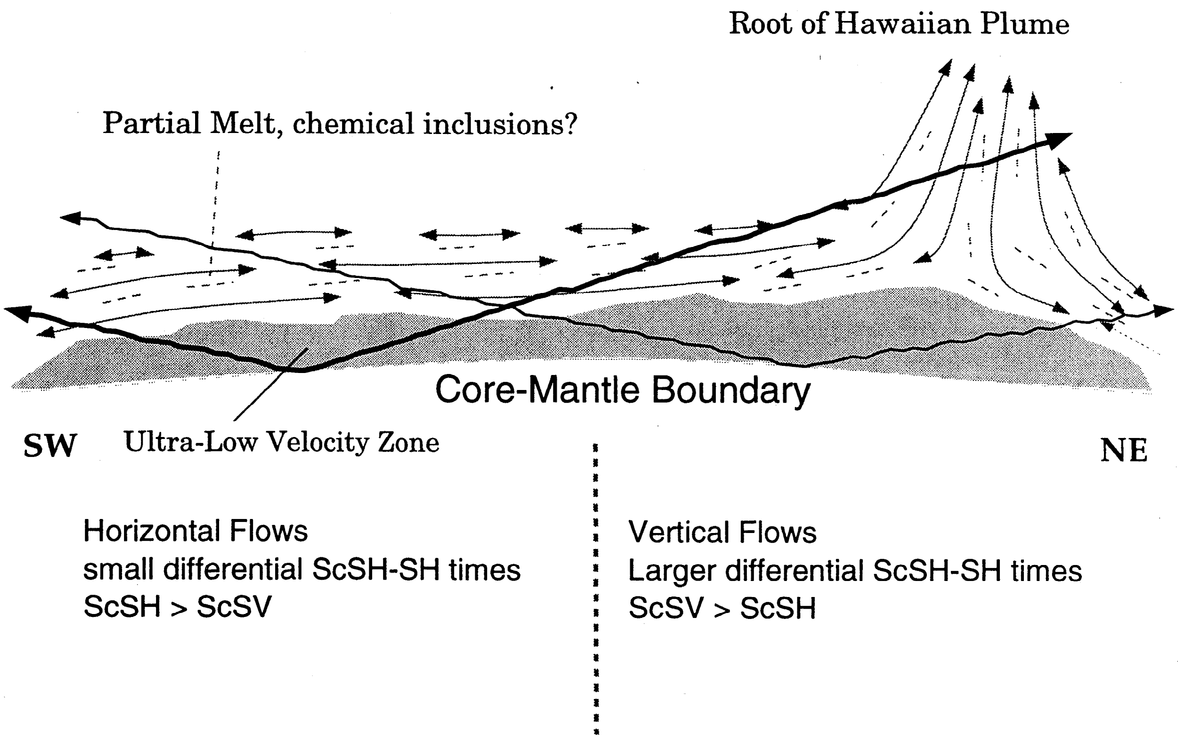

Figure 18. A drawing of the boundary layer at the CMB that summarizes the observed differential travel time and anisotropy observations. Differential shear flows that upwell into a mantle plume in the northeast affect ray paths differently depending on what region they sample. *ScS* reflecting in the southwestern region (left) would have *ScSH* travel faster than *ScSV* due to the horizontally sheared structure with embedded partial melt, while in the northeastern region (right), *ScSV* will travel faster than *ScSH* due to vertically sheared fabric of partial melt and chemical heterogeneity.

dynamic regime is indicated by our data to be on the scale of 500-600 km, whatever the precise mechanism.

Given the proximity of this D" region to Hawaii, it is possible that this convective upwelling is related to the mantle plume feeding the hotspot. Because of the theorized small diameter of the plume conduit at depth in the mantle, conjectured to be approximately 70-180 km at the CMB for the Hawaii plume [*Duncan and Richards*, 1991; *Griffiths and Campbell*, 1991], it is very difficult to find source-receiver geometries that can directly detect mantle plumes. There have been several recent studies that attempt to image mantle plumes. *Nataf and VanDecar* [1993] present evidence for detection of the mantle plume feeding the Bowie hotspot in Canada at a depth of approximately 700 km based on travel time analyses. Recently, *Ying and Nataf* [1997] used diffraction tomography to image an anomalous feature at the base of the mantle northwest of the Hawaiian islands. However, *Steinberger and O'Connell* [1998] propose that Hawaii's plume source is located to the southeast of Hawaii based on convective modeling using seismic tomography models to define density heterogeneity and associated mantle shear flow. Their location of the Hawaiian plume at the CMB is precisely in the region sampled by the ray paths in this study (ellipse in Figure 9). In order to assess the possibility that we are imaging a convective feature at the base of the mantle, additional ray sampling to the northeast is needed. This will be difficult to achieve using *ScS* phases as they converge with direct *S*; however, a combination of shear phases may be considered.

7. Conclusion

Analysis of an extensive shear wave data set that samples the D" region beneath the central Pacific reveals that *ScS* travel times are 3-5 s slower for model PREM indicative of significantly slower than average structure. There is evidence for the presence of laterally varying anisotropy from observations of *ScS* splitting. Mapping the *ScSH-SH* differential times and the anisotropy measurements at their CMB reflection points reveals small-scale gradients with smaller differential times and *ScSH* advances relative to *ScSV* in the southwest of the region to larger differential times and *ScSV* advances relative to *ScSH* in the northeast region. We interpret these trends to be created by a gradient in boundary layer shear flow, possibly containing chemical or melt heterogeneities, from horizontal flow in the southwest to upwelling flow in the northeast. If this anomalous zone is restrained to the lowermost 250 km of the mantle, this requires 2-3% anisotropic gradients, with a 90° rotation of fast polarization, and a 3.5% variation in shear velocity over length scales of 500-600 km. The close proximity of the study region to the proposed location of the base of the Hawaiian plume raises the possibility that the gradient in structure reflects inflow and ascent of material feeding the plume.

Acknowledgments. We thank B. Steinberger for providing a preprint and plume locations, R. Hartog for assistance with measuring anisotropy, and S. Grand for providing his 3-D tomographic model. We also thank the two anonymous reviewers and the Associate Editor for their comments on the manuscript. We used the GMT mapping software by *Wessel and Smith* [1991] to prepare many of the figures. Data were obtained through the IRIS Data Management System. This research was supported by NSF grants EAR 9418643 (T.L) and EAR 989604 (E.J.G.). Contribution 351 of the Institute of Tectonics and the W.M. Keck Seismological Laboratory.

References

Ansel, V., and H.-C. Nataf, Anisotropy beneath nine stations of the Geoscope broadband network as deduced from shear-wave splitting, *Geophys. Res. Lett., 16,* 409-412, 1989.

Bataille, K., S. Wu, and S.M. Flatte, Inhomogeneities near the core-mantle boundary evidenced from scattered waves: A review, *Pure Appl. Geophys., 132,* 151-174, 1990.

Ding, X., and D.V. Helmberger, Modeling D" structure beneath Central America with broadband seismic data, *Phys. Earth Planet. Int., 101,* 245-270, 1997.

Duncan, R.A., and M.A. Richards, Hotspots, mantle plumes, flood basalts, and true polar wander, *Rev. Geophys., 29,* 31-50, 1991.

Dziewonski, A.M., and D.L. Anderson, Preliminary reference Earth model (PREM), *Phys. Earth Planet. Inter., 25,* 297-356, 1981.

Fischer, K.M., and D. Wiens, The depth distribution of mantle anisotropy beneath the Tonga subduction zone, *Earth Planet Sci. Lett., 142,* 253-260, 1996.

Gaherty, J.B., and T. Lay, Investigation of laterally heterogeneous shear velocity structure in D" beneath Eurasia, *J. Geophys. Res., 97,* 417-435, 1992.

Garnero, E.J., D.V. Helmberger, and G. Engen, Lateral variations near the core-mantle boundary, *Geophys. Res. Lett., 15,* 609-612, 1988.

Garnero, E.J., and D.V. Helmberger, Preliminary evidence for a lower mantle shear wave velocity discontinuity beneath the central Pacific, *Phys. Earth Planet. Int., 79,* 335-347, 1993.

Garnero, E.J., and D.V. Helmberger, Seismic detection of a thin laterally varying boundary layer at the base of the mantle beneath the central Pacific, *Geophys. Res. Lett., 23,* 977-980, 1996.

Garnero, E.J., and T. Lay, Lateral variations in lowermost mantle shear wave anisotropy beneath the north Pacific and Alaska, *J. Geophys. Res., 102,* 8121-8135, 1997.

Grand, S.P., R.D. van der Hilst, and S. Widiyantoro, Global seismic tomography: A snapshot of convection in the Earth, *GSA Today, 7,* 1-7, 1997.

Griffiths, R.W., and I.H. Campbell, On the dynamics of long-lived plume conduits in the convecting mantle, *Earth Planet. Sci. Lett., 103,* 214-227, 1991.

Holland, K.G., and T.J. Ahrens, Melting of $(Mg,Fe)_2SiO_4$ at the core-mantle boundary of the Earth, *Science, 275,* 1623-1625, 1997.

Karato, S.-I., Some remarks on the origin of seismic anisotropy in the D" layer, *Earth, Planets and Space, 50,* 1019-1028, 1998.

Kendall, J.M., and P.G. Silver, Constraints from seismic anisotropy on the nature of the lowermost mantle, *Nature, 381,* 409-412, 1996.

Knittle, E., and R. Jeanloz, Earth's core-mantle boundary: Results of experiments at high pressures and temperatures, *Science, 251,* 1438-1443, 1991.

Kuo, B.-Y., and K.-Y. Wu, Global shear velocity heterogeneities in the D" layer: Inversion from Sd-SKS differential travel times, *J. Geophys. Res., 102,* 11775-11788, 1997.

Lavely, E.M., D.W. Forsyth, and P. Friedmann, Scales of heterogeneity near the core-mantle boundary, *Geophys. Res. Lett., 13,* 1505-1508, 1986.

Lay, T., Localized velocity anomalies in the lower mantle, *Geophys. J. R. Astro. Soc., 72,* 483-516, 1983.

Lay, T., and D.V. Helmberger, A lower mantle S-wave triplication and the shear velocity structure of D", *Geophys. J. R. Astr. Soc., 75,* 799-837, 1983.

Lay, T., E.J. Garnero, C. Young, and J.B. Gaherty, Scale-lengths of shear velocity heterogeneity at the base of the mantle from S wave differential travel times, *J. Geophys. Res., 102,* 9887-9909, 1997.

Lay, T., Q. Williams, and E.J. Garnero, The core-mantle boundary layer and deep earth dynamics, *Nature, 392,* 461-468, 1998a.

Lay, T., Q. Williams, E.J. Garnero, L. Kellogg, and M. Wysession, Seismic wave anisotropy in the D" region and its implications, in *The Core Mantle Boundary, Geodyn. Ser.*, vol. 28, edited by M. Gurnis et al., pp. 299-318, American Geophysical Union, Washington, D.C., 1998b.

Li, X.D., and B. Romanowicz, Global mantle shear velocity model developed using nonlinear asymptotic coupling theory, *J. Geophys. Res., 101,* 22245-22272, 1996.

Loper, D.E., and T. Lay, The core-mantle boundary region, *J. Geophys. Res., 100,* 6397- 6420, 1995.

Masters, T.G., S. Johnson, G. Laske, and H. Bolton, A shear-velocity model of the mantle, *Philos. Trans. Soc. London, 354,* 1385-1411, 1996.

Matzel, E., M.K. Sen, and S.P. Grand, Evidence for anisotropy in the deep mantle beneath Alaska, *Geophys. Res. Lett., 23,* 2417-2420, 1996.

Menke, W., Few 2-50 km corrugations on the core-mantle boundary, *Geophys. Res. Lett., 13,* 1501-1504, 1986.

Mori, J., and D.V. Helmberger, Localized boundary layer below the mid-Pacific velocity anomaly identified from a PcP precursor, *J. Geophys. Res., 100,* 20359-20365, 1995.

Murphy, F.E., J.W. Neuberg, and A.W.B. Jacob, Alternatives to core-mantle boundary topography, *Phys. Earth Planet. Inter., 103,* 349-364, 1997.

Nataf, H.-C., and J. VanDecar, Seismological detection of a mantle plume?, *Nature, 364,* 115-120, 1993.

Neuberg, J., and T. Pointer, Modelling seismic reflections from D" using the Kirchoff method, *Phys. Earth Planet. Inter., 90,* 273-281, 1995.

Olson, P., G. Schubert, and C. Anderson, Plume formation in the D"-layer and the roughness of the core-mantle boundary, *Nature, 327,* 409-413, 1987.

Pulliam, J., and M.K. Sen, Seismic anisotropy in the core-mantle transition zone, *Geophys. J. Int., 135,* 113-128, 1998.

Reasoner, C., and J.S. Revenaugh, Short-period *P* wave constraints on D" reflectivity, *J. Geophys. Res., 104,* 955-962, 1999.

Revenaugh, J.S., and R. Meyer, Seismic evidence of partial melt within a possibly ubiquitous low velocity layer at the base of the mantle, *Science, 277,* 670-673, 1997.

Ritsema, J., E.J. Garnero, and T. Lay, A strongly negative shear velocity gradient and lateral variability in the lowermost mantle beneath the Pacific, *J. Geophys. Res., 102,* 20395-20411, 1997.

Ritsema, J., T. Lay, E.J. Garnero, and H. Benz, Seismic anisotropy in the lowermost mantle beneath the Pacific, *Geophys. Res. Lett., 25,* 1229-1232, 1998.

Russell, S.A., T. Lay, and E.J. Garnero, Seismic evidence for small-scale dynamics in the lowermost mantle at the root of the Hawaiian hotspot, *Nature, 396,* 255-258, 1998.

Savage, M.K., P.G. Silver, and R.P. Meyer, Observations of teleseismic shear-wave splitting in the Basin and Range from portable and permanent stations, *Geophys. Res. Lett., 17,* 21-24, 1990.

Silver, P.G., Seismic anisotropy beneath the continents: Probing the depths of geology, *Ann. Rev. Earth Planet. Sci., 24,* 385-432, 1996.

Silver, P.G., and W.W. Chan, Shear wave splitting and subcontinental mantle deformation, *J. Geophys. Res., 96,* 16429-16454, 1991.

Sleep, N.H., Gradual entrainment of a chemical layer at the base of the mantle by overlying convection, *Geophys. J., 95,* 437-447, 1988.

Stacey, F.D., and D.E. Loper, The thermal boundary-layer interpretation of D" and its role as a plume source, *Phys. Earth Planet. Int., 33,* 45-55, 1983.

Steinberger, B., and R.J. O'Connell, Advection of plumes in mantle flow: Implications for hotspot motion, mantle viscosity and plume distribution, *Geophys. J. Int., 132,* 412-434, 1998.

Su, W.-J., R. Woodward, and A.M. Dziewonski, Degree 12 model of shear velocity heterogeneity in the mantle, *J. Geophys. Res., 99,* 6945-6980, 1994.

Tanimoto, T., Long-wavelength S-wave velocity structure throughout the mantle, *Geophys. J. Int., 100,* 327-336, 1990.

Vinnik, L., B. Romanowicz, Y. Le Stunff, and L. Makeyeva, Seismic anisotropy in the D" layer, *Geophys. Res. Lett., 22,* 1657-1660, 1995.

Vinnik, L., L. Breger, and B. Romanowicz, Anisotropic structures at the base of the Earth's mantle, *Nature, 393,* 564-567, 1998.

Weber, M., P and S reflections from anomalies in the lowermost mantle, *Geophys. J. Int., 115,* 183-210, 1993.

Weber, M., and J.P. Davis, Evidence of a laterally variable lower mantle structure from P- and S-waves, *Geophys. J. Int., 102,* 231-255, 1990.

Wessel, P., and W.H.F. Smith, Free software helps map and display data, *EOS, 72,* 441,445-446, 1991.

Williams, Q., and E.J. Garnero, Seismic evidence for partial melt at the base of Earth's mantle, *Science, 273,* 1528-1530, 1996.

Woodward, R.L., and G. Masters, Lower-mantle structure from ScS-S differential travel times, *Nature, 352,* 231-233, 1991.

Wysession, M.E., Continents of the core, *Nature, 381,* 374-375, 1996.

Wysession, M.E., L. Bartko, and J.B. Wilson, Mapping the lowermost mantle using core- reflected shear waves, *J. Geophys. Res., 99,* 13667-13684, 1994.

Ying, J., and H.-C. Nataf, Detection of mantle plumes in the lower mantle by diffraction tomography: Hawaii, *Earth Planet. Sci. Lett., 159,* 99-115, 1997.

Young, C., and T. Lay, Evidence for a shear velocity discontinuity in the lowermost mantle beneath India and the Indian Ocean, *Phys. Earth Planet. Int., 49,* 37-53, 1987.

Zhang, J., and T. Lay, Investigation of a lower mantle shear wave triplication using a broadband array, *Geophys. Res. Lett., 11,* 620-623, 1984.

E.J. Garnero, Department of Geology, Arizona State University, Box 871404, Tempe, AZ 85287. (garnero@asu.edu)

T. Lay, S. A. Russell, Earth Sciences Department and Institute of Tectonics, University of California, Santa Cruz Santa Cruz, CA 95064.
(tlay@es.ucsc.edu; sara@es.ucsc.edu)

(Received September 15, 1998; revised February 3, 1999; accepted March 1, 1999.)